

By the end of the first report period we had realized that problems arose with the affinity purification and the ascorbate (ASC) reducibility of the heterologously expressed mouse tumor suppressor cytochrome *b561* protein (MmCYB561D2) when a Strep-II tag was present on its C-terminus. The yield of the protein also remained rather low. The length of the linker sequence connecting the Strep-II tag to the protein C-terminus did not affect these findings. We continued to test our hypothesis that the Strep-II tag could specifically interact with the cytoplasmic ascorbate binding site and/or the cytoplasmic side heme, in case of the tumor suppressor protein. Deleting the C terminal Strep-II tag together with the thrombin cleavage site from the gene of MmCYB561D2 led to the recovery of the ascorbate reducibility, as measured on the membrane fraction and on the detergent solubilized fraction. Since the variant with the C terminal thrombin cleavage site and His₆ tag can be readily purified and reduced by ASC, it is the Strep-II tag itself that must interfere with the ascorbate reducibility. The codon optimized *Arabidopsis thaliana* tonoplast cytochrome *b561* (AtCYB561B1) gene has been expressed in the same expression system and, – unlike the tumor suppressor protein –, this protein could be purified with the Strep-tactin affinity resin and retained the ascorbate reducibility.

We have inserted the internal His₆ and Strep-II tags in the 1st and 5th interhelix loops of MmCYB561D2 (both loops on the non-cytoplasmic side of the protein) to facilitate affinity purification either in the presence or in the absence of the C terminal Strep-II tag. Purification was successful with the loop-inserted His₆ affinity tags (which is a non-trivial result), while the presence of the C-terminal Strep-II tag still almost completely prevented the purified protein's reduction by ascorbate.

MmCYB561D2 variants:
Strep-II tagged, untagged,
His-tagged in 1st and in 5th
interloop.



 TSCyt-*b561*
 heme-*b* center
 Internal His-tag
 Thrombin site
 Strep-II tag

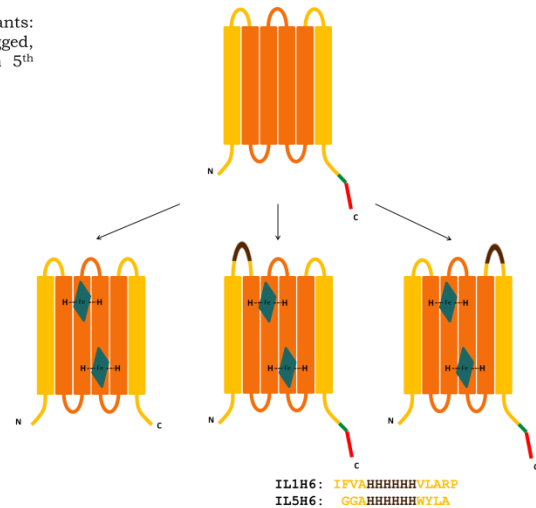


Figure 1.

We have established an expression system for cytochrome *b561* proteins in *Pichia pastoris* cells as well. In the third period we constructed several variants of the so far never studied MmCYB561D1 (a close homologue of the tumor suppressor CYB561D2), whose expression and purification opened the way towards the determination of various properties of this novel member of the CYB561 family. Accordingly, the following constructs have been made in the second and third periods:

- yeast host codon optimized tumor suppressor MmCYB561D2 with no tag, in the *Saccharomyces cerevisiae* strain yTHCBMS1, reported optimal for membrane protein expression

- 4 constructs with the codon optimized, C-terminal thrombin cleavage site + Strep-II tag-fused gene of the MmCYB561D2 protein with either Strep-II or His₆ tag in the 1st or 5th interhelical loops, in yTHCBMS1
- MmCYB561D2 gene with a His₆ tag in either the 1st or the 5th interhelical loop, but no fusion peptide on the C terminus, in yTHCBMS1
- codon optimized double mutant (HHAA in the putative 2nd and 4th transmembrane helix) MmCYB561D2 gene with His₆ tag on the C terminus
- native codon double mutant (HHAA in the putative 2nd and 4th transmembrane helix) MmCYB561D2 gene with His₆ tag on the C terminus
- as a control, codon optimized, C-terminal thrombin cleavage site + Strep-II tag-fused gene of the *Arabidopsis thaliana* tonoplast cytochrome *b561* (AtCYB561B1) protein in yTHCBMS1
- codon optimized MmCYB561D2 without tags in the *Pichia pastoris* yeast strain KM71
- codon optimized MmCYB561D2 with C-terminal thrombin cleavage site and Strep-II tag in the *Pichia pastoris* strains GS115 and KM71
- codon optimized MmCYB561D2 with C-terminal thrombin cleavage site and His₆ tag in the *Pichia pastoris* strains GS115 and KM71
- codon optimized AtCYB561B1 with C-terminal thrombin cleavage site and Strep-II tag in the *Pichia pastoris* strains GS115 and KM71
- codon optimized MmCYB561D1 with C-terminal thrombin cleavage site and His₆ tag in yTHCBMS1
- codon optimized single mutant (HA in the putative 2nd or 4th transmembrane helix) MmCYB561D1 with C-terminal thrombin cleavage site and His₆ tag in yTHCBMS1
- codon optimized double mutant (HHAA in the putative 2nd and 4th transmembrane helix) MmCYB561D1 with C-terminal thrombin cleavage site and His₆ tag in yTHCBMS1

In our continued efforts to optimize the yield of purified, functional CYB561 proteins we have compared the output of the *Saccharomyces* and the *Pichia* expression systems. So far the *Pichia* strains have been in fact inferior to the *Saccharomyces* strains.

The circular dichroism spectrum of purified WT AtCYB561B1 in the Soret region showed typical excitonic splitting with almost perfectly symmetrical positive/negative lobes, and bipolar excitonic splitting was also discernible, although at a much smaller amplitude, in the visible (alpha) band (Fig. 2). This is a clear indication of the electronic interaction of the two hemes and, also, of the integrity of the protein with close to full occupancy of both heme binding pockets. The excitonic features disappeared in double mutants containing only one heme. CD spectra on WT MmCYB561D2 have also shown an excitonic contribution in the Soret region both in the reduced and in the oxidized form of the protein. This was, however, rather asymmetrical. Together with the fact that the 415 nm (Soret) to 280 nm (protein) absorption ratio was unusually low, this could indicate that in only a fraction of the protein are both heme centers present, and there is a sizeable population with only one bound heme. In the presumably intact proteins,

though, the electronic interaction between the hemes was clearly observable, just like in the tonoplast protein. However, in the highly homologous MmCYB561D1 protein there was virtually no sign of excitonic interaction between the hemes (Fig. 2). An indirect proof of the presence of both hemes (at least in the overwhelming majority of the protein population) could be derived from the biphasic titration with ascorbate, a typical result for other, better characterized family members, that is usually explained by two ASC binding sites communicating with the two hemes individually (Fig. 3).

Expression of the double HHAA mutant and single HA mutant MmCYB561D1 proteins, where the histidines are the ones on helices 2 and 4, coordinating the cytoplasmic side heme (assignment based on homology modeling, see later), yielded very low amounts of the purified proteins and no ASC reducibility. Nevertheless, the proteins were identified by Western blot. These data indicate that the non-cytoplasmic side heme – at least in this protein – can only be reduced by ascorbate from the cytoplasmic side and indirectly, by the reduced cytoplasmic side heme.

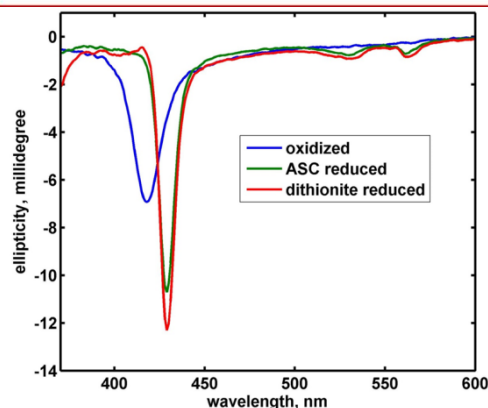
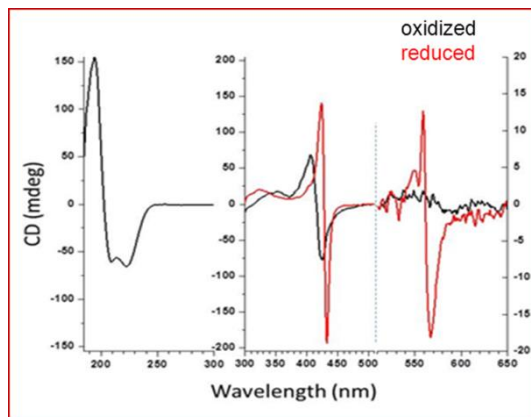


Figure 2. CD spectra of oxidized and reduced AtCYB561B1 (top) and MmCYB561D1 (bottom).

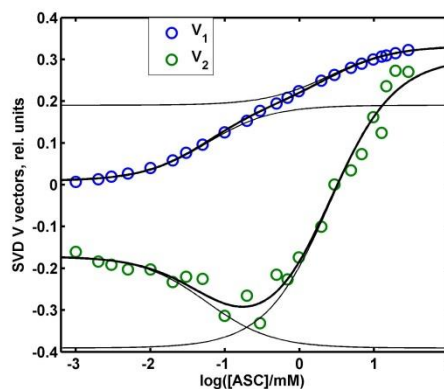
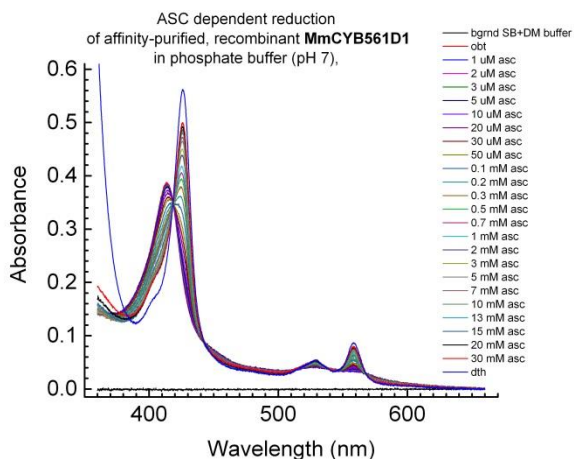


Figure 3. ASC titration of MmCYB561D1

Redox titration of the purified MmCYB561D1 protein resulted in two clearly distinct midpoint redox potentials, also indicating the presence of both hemes (Fig. 4). The separation of the two midpoint redox potentials (160 mV) is significantly larger than in other members of the protein

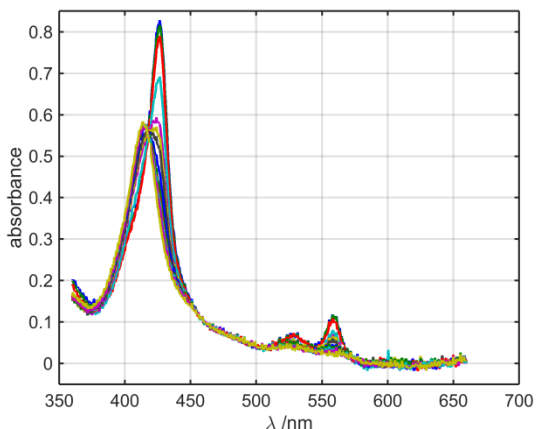
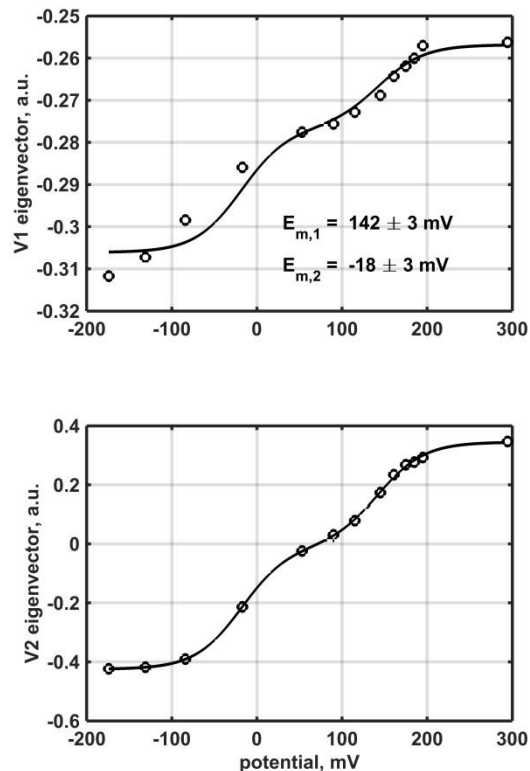


Figure 4. Redox titration MmCYB561D1



family (usually ~ 100 mV). Spectra were globally analysed by singular value decomposition and both here and in the case of the ascorbate titration above, 2 significant spectral eigenvectors were found, in variance with the plant AtCYB561B1 and the mouse TSCYB561D2, where the spectral matrices were rank 3, indicating a spectral difference between the two hemes' reduced forms.

Low temperature continuous wave electron paramagnetic resonance (EPR) spectra taken on oxidized and $\sim 50\%$ reduced (i.e. one heme already reduced, the other one still oxidized) MmCYB561D1 protein are very similar to those obtained by others for the tumor suppressor HsCYB561D2, but different from other CYB561 proteins. No EPR signal is apparent around $g_z = 3.15$ and the signal at $g_z = 3.71$ significantly decreases after about 50% reduction of MmCYB561D1 as it is shown in Fig. 5, and a less intense signal becomes

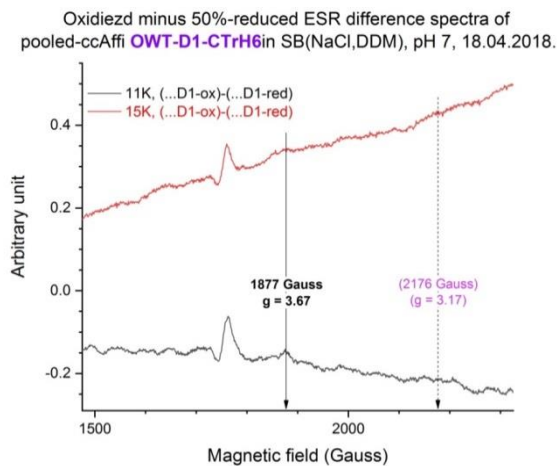


Figure 5. EPR signals of MmCYB561D1.

visible at $g_z = 3.67$. The intensity of this latter signal decreases with increasing the temperature from 11 K to 15 K. Thus it seems that in MmCYB561D1 the two hemes have a highly asymmetric low-spin (HALS) character.

Altogether, the optical (CD, ascorbate and redox titration UV-vis) and EPR spectroscopic findings show that the interaction of the hemes with the protein environment and, perhaps, also the position/orientation of the hemes in MmCYB561D1 might be slightly different from those in the other members of the cytochrome *b561* protein family.

A novel vitamin E (tocopherol) analogue was provided to us by foreign partners to test its interaction with cytochrome *b561* proteins. Our experiments have shown that this lipophilic compound appeared to oxidize the reduced AtCYB561B1 or, more precisely, appeared to accelerate the autooxidation of the protein. It did not interact with the oxidized form of the protein. As a control, alpha-tocopherol itself (the parent compound) did not alter the autooxidation rate. In other words, the effect of this vitamin E analogue seems to be opposite to that of vitamin C (ascorbate), the general electron donor of the cytochrome *b561* proteins. These results were presented in a poster at the domestic Sümeg conference, but not published due to an unresolved conflict with the foreign partner about the interpretation.

We have performed homology modeling of the structure of 10 CYB561 proteins based on the single available crystal structure of the plant AtCYB561B2 family member – whose function is unknown (Table 1). (Very recently another crystal structure was published. Our preliminary results show that the model structures obtained from this second crystal structure as template are very similar to the structures obtained from the first crystal structure.)

protein	abbreviation	Sequence identity ¹ with AtCYB561B2, %
Arabinopsis thaliana tonoplast	AtCYB561B1	43
Zea mays tonoplast	ZmCYB561B1	42
Bos Taurus chromaffin granule	BtCYB561A1	34
Mus musculus chromaffin granule	MmCYB561A1	34
Mus musculus duodenal	MmCYB561A2	31
Mus musculus lysosomal	MmCYB561A3	34
Mus musculus tumor suppressor	MmCYB561D2	21
Mus musculus, unknown	MmCYB561D1	22
Homo sapiens duodenal	HsCYB561A2	34
Homo sapiens tumor suppressor	HsCYB561D2	20

Table 1. Proteins involved in homology modeling, their abbreviated name and the percentage of their sequence identity with the crystallized AtCYB561B2 protein. In the sequence alignment the N and C terminal regions corresponding to the N and C terminal sequences of AtCYB561B2 missing from the crystal structure were not included. ¹percentage of identical amino acids in the alignment, percentage of homology was much higher in all cases.

Comparing the location of particular amino acid residues in the homology model structures with the predicted effects of point mutations deduced from experimental results has revealed a need for immediate correction in the structure-function relations; in particular in case of interpreting the reduction of CYB561 proteins by ascorbate. The systematic comparison of published experimental results obtained on numerous site directed mutants of various cytochrome *b*561 proteins with their homology modeled structure is still under way. In particular, we have modeled the position in AtCYB561B1 of the five conserved lysine residues (K70, K76, K79, K80, K149), which had earlier been experimentally replaced by alanine, leading to various altered properties. These are all close to the cytoplasmic ascorbate binding site, but our model shows that most of them do not participate directly in the binding. Interestingly, replacement of K70, which in the model interacts with the propionate side chain of the high potential heme *b*, results in a substantial decrease of the ascorbate concentration required for a 50% reduction of this heme. On the other hand, replacement of K80, a lysine directly involved in the cytoplasmic side ascorbate binding according to our homology model, affected the properties of the distant, non-cytoplasmic, low potential heme: for the 50% reduction of the latter, substantially higher ascorbate concentrations were necessary. In order to understand these experimental results a reaction model accounting for the two hemes and the (at least) two ascorbate binding sites on the opposite membrane surfaces and their mutual interactions will be necessary.

We have also performed docking calculations of ASC and of monodehydroascorbate (MDA) to both sides of the experimentally determined and the homology modeled structures of the CYB561 proteins. Our goal in these studies is primarily to characterize the non-cytoplasmic side docking – or the lack thereof – that could provide information regarding the substrate of the various proteins on this side. On the non-cytoplasmic side the ASC ligand found in the crystal structure was stabilized by hydrogen bonds to the side chains of His106, Tyr115 and Asn186, and by pi-pi stacking interactions with Phe105 and Phe182. None of these residues are highly conserved, indicating that, as expected, MDA is not always the physiological oxidant on the non-cytoplasmic side. In

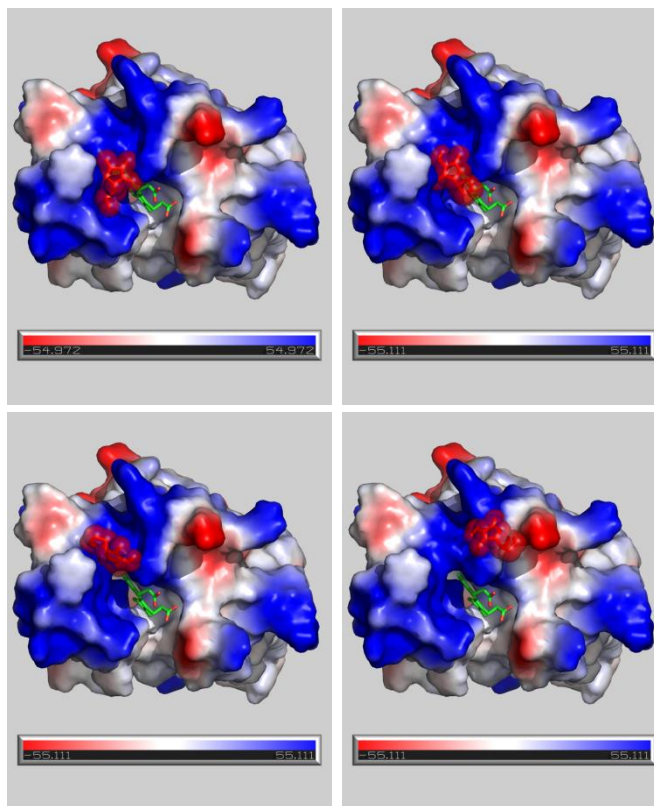


Figure 6. Homolgy modeled and the 3 docking poses of ASC at the cytoplasmic side of the bovine chromaffin granule protein (BtCYB561A1) clockwise from top left.

addition, the protein surface on the non-cytoplasmic side appears to be less positively charged than the cytoplasmic surface. We have used the available AtCYB561B2 crystal structure and our modeled structures to study the interaction of the ASC and MDA substrates with these proteins. In particular, in addition to crystallized AtCYB561B2, modeled BtCYB561A1 (Fig. 6), AtCYB561B1, MmCYB561D1 and MmCYB561D2 structures were investigated. We have identified potential binding sites by docking calculations on both water exposed sides, performed cluster analysis of the multitude of substrate positions to obtain representative conformations of the docked substrates and the proteins, and calculated the stabilizing intermolecular interactions between them. Several docking positions were obtained on both sides of the proteins as the docking was primarily governed by the sizable positive electrostatic patches on the surfaces exposed to the aqueous phases. The bound ligands established also varying hydrogen bonding interactions with protein side chains. No single, dominant position was found, suggesting that ASC can probably reduce (and MDA can oxidize, if it is the oxidant) CYB561 proteins without true ligand binding, primarily via loose electrostatic encounter. This contradicts the two crystal structures, where ASC was found at the same well defined site in both cases. Nevertheless, ASC was added by soaking the crystals in ASC containing media and we assume that in the crystal only limited access is possible for the ligand to the surfaces of the proteins.

We have calculated electron transfer pathways (pathway model) and efficiencies (packing density model) in the crystallographically determined (Fig. 7) and in the homology modeled cytochrome b561 structures from cytoplasmic ASC to non-cytoplasmic MDA via the two hemes. The distance between the substrates and the corresponding hemes is so short that the most efficient route is a single through space jump for the electron. Between the two hemes the optimal pathway includes several covalent, H-bond and through space jumps, it may involve an internal water molecule, but varies from protein to protein. This is because there is no conserved amino acid in this region, so it appears that a sufficient packing density is the only requirement for the efficient electron transfer between the hemes.

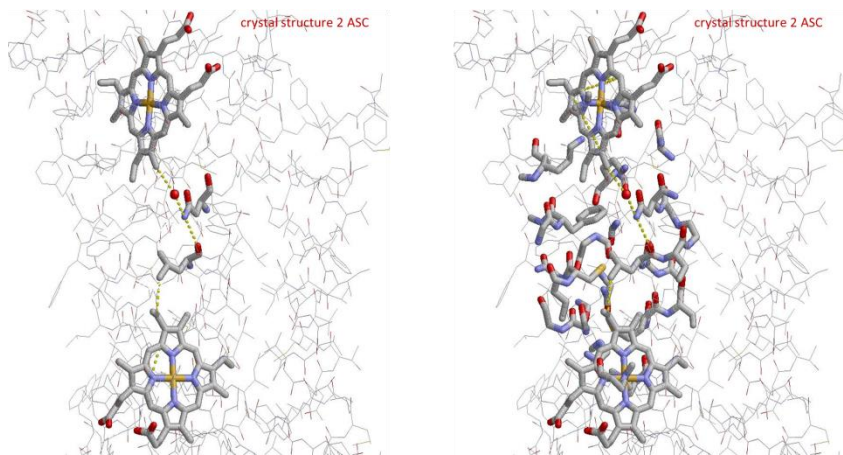


Figure 7. The kinetically most probable electron transfer pathway (left) and residues between the two heme-b centers in the crystal structure of AtCYB561B2 which might participate in electron transfer with almost the same efficiency (right).

To further optimize the production of purified CYB561D1 we have tested several detergents. Among the non-ionic n-dodecyl- β -D-maltoside (DDM), Triton X-100R and C12E8 and the zwitterionic SB-3-14 and SB-3-16, it was the dodecyl maltoside that gave the highest yield of solubilized and ASC reducible protein. Very recently, a detergent-free method of isolating membrane proteins in lipid nanodisks is becoming more and more popular. This is based on the styrene-maleic acid (SMA) copolymers, that are polyelectrolyte amphiphilic molecules, and its advantage is that – if successful – it leaves the protein in its native lipid environment. In collaboration with the University of Szeged we have performed experiments with the SMA method as an alternative to the less native (and more expensive) detergent solubilisation.

SMA molecules can create *micro*-domains in which integral membrane proteins are kept together with their surrounding lipids. As it can be deduced from the few publications in this field until now, application of SMA molecules with different styrene to maleic acid ratio ($N_S:N_{MA}$) as well as with different polymerization degree (final molecular mass) might result in different success in case of different *trans*-membrane proteins. SMA(2:1) and SMA(3:1) copolymers with molecular mass between 3,000 and 10,000 Da are the two most frequently used SMA copolymers. However, no systematic study has appeared so far to compare the efficiency of these two (and other) copolymers in membrane-protein nanodisc preparation. In order to improve our solubilisation yield and to test whether some SMA copolymers are capable of solubilizing CYB561 proteins, we have compared the parameters of solubilized particles obtained by using SMA(2:1), SMA(3:1), SMA(1:2) copolymers and DDM for disintegrating the yeast microsomal membrane fraction of cells heterologously expressing the recombinant MmCYB561D1 protein.

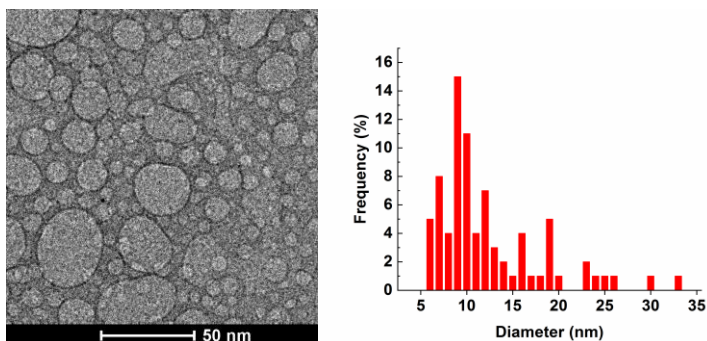


Figure 8. TEM pictures after solubilization/dismantling of yeast microsomal membrane fraction by SMA(2:1) and the histogram of particles.

The particle sizes obtained after the solubilization of the yeast microsomal membrane fraction by DDM or SMA copolymers were determined by transmission electron microscopy (TEM, Fig. 8) and differential light scattering (DLS) measurements as well. Besides the population with size distribution seen in the TEM image DLS also detected another population at about 100 nm, that may be nanodisk aggregates or lipid nanodisks harboring larger protein clusters or complexes.

The results obtained by UV/Vis spectroscopy, dynamic light scattering technique, atomic force and transmission microscopy have allowed us to claim that (1) SMA(2:1) is as efficient as DDM and 2-3 times more efficient than SMA(3:1), (2) SMA(X:1) copolymers used (X=1/2,2,3) highly affect the interaction of the proteins in *micro*-domains with negatively charged substrates, such

as ascorbate, and (3) the size of particles obtained by different solubilizing agents are very inhomogeneous. Due to the rather high negative charge density on SMA copolymers, these agents are not recommended to be used when the goal is to study the function of an integral membrane protein in nanoparticles that functions with negatively charged substrate(s).

We have also performed a thorough lipidomic analysis of the SMA nanodisks and DDM nanoparticles to find out any preference/selectivity depending on the membrane dismantling agent (Fig. 9). The GPL/prot of the nanodisks was strongly dependent on the linear charge density of the SMA copolymers applied. The lipid composition of the DDM-solubilized bicelles was strongly dependent on the ionic

strength of the solubilization buffer; the higher the ionic strength the lower the amount of lipids in the solubilized particles. Numerous significant differences were found throughout the lipidome, which altogether point to the different selectivities of the applied dismantling agents. Since the GPL components play an important role in preserving the activity of many transmembrane proteins, both the qualitative and the quantitative characterization of the GPL composition of nanoparticles obtained after biomembrane dismantling by SMA copolymers may provide valuable information. Thus, our results might be important in future applications of the SMA copolymers as well as DDM for studying the properties of integral membrane proteins.

With the SMA system in our hands, we carried out a somewhat independent study in collaboration with the University of Szeged that led to a potential pharmaceutical application of these co-polymers. We have evaluated the pH- responsive SMA nanoparticles for the encapsulation and intelligent drug release ability of the poorly water soluble model drug, ketoprofen. Increasing styrene content of the copolymer led to lower surface charge (from -28.4 to -15.0 meq/100 g) and the different styrene/ maleic acid ratio (1:2, 2:1 and 3:1) influences the pH- dependent solubility properties. Because of the polyanionic nature, homogeneous polymer solution was obtained at higher pH, while at lower pH nanoparticles were formed. The corresponding cut-off pH values showed increasing tendency with increasing hydrophobicity (pH= 3.12, 4.22 and 5.44 for 1:2, 2:1 and 3:1, respectively).

The hydrophobic, non- water soluble KETO drug was coated with SMA(2:1) shell. The polymer-stabilized KETO particles formed stable dispersion in aqueous environment, i.e. the prepared polymer shell increased the water dispersibility of the initially hydrophobic drug. According to the experiments the release of low crystallinity KETO drug was almost complete at physiological

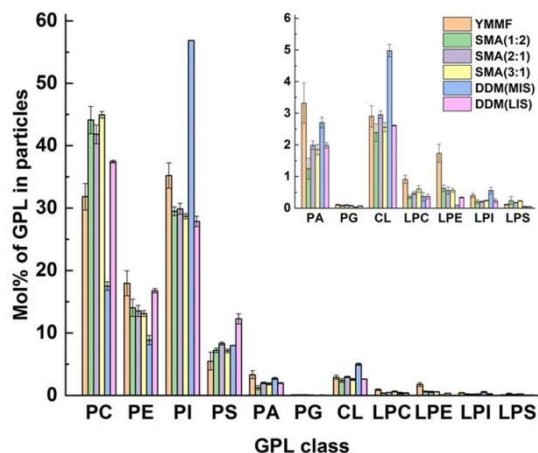


Figure 9. Major and minor (inset) GPL components (lipid classes; expressed as mol% of total GPL) in the particles obtained after solubilization of the yeast microsomal membrane fraction.

pH (=7.4), while at acidic pH the released amount of the model drug was only about 30%. The prepared NPs could be useful in all areas where the alkaline pH value causes problems, for example in the case of female genital diseases of fungal origin.

The autocatalytic enzymatic reactions have been studied by one of the senior participants (Csaba Bagyinka) in another redox protein, the HynSL hydrogenase from *Thiocapsa roseopersicina*. In this protein electron and proton transfer events are coupled to the reversible oxidation of molecular hydrogen by an oxidizing agent:



A model has been built to describe the hydrogenase catalyzed, autocatalytic, reversible hydrogen oxidation reaction where one of the enzyme forms is the autocatalyst. The model not only reproduces the experimentally observed reaction front properties in both well stirred and spatially confined (2 dimensional) reaction vessels, but also explains the hydrogen ion dependence of the front velocities and spatial patterns in the wide pH range of 2-10. Furthermore, by linear stability analysis, two different front types were found in good agreement with the experiments. The results reveal that the characteristic time scales of the autocatalysis and the reduction of the electron acceptor are responsible for the dual features of the reaction: at large substrate excess, the time scales match, resulting in the expression of its autocatalytic nature, allowing the appearance of reaction fronts, while at lower substrate excess, the autocatalytic enzyme activation remains invisible and the conversion of the electron acceptor follows a regular lag phase with no reaction-diffusion front evolution.